AGU PUBLICATIONS

JGR

Journal of Geophysical Research: Space Physics

RESEARCH ARTICLE
10.1002/2015JA021535

Key Points:
- Magnetic reconnection regions should manifest themselves as loads (power density $\mathbf{E} \cdot \mathbf{J} > 0$)
- We show that an event with power density $\gtrsim$20 pW/m^3 is likely to be associated with tail reconnection
- $\mathbf{E} \cdot \mathbf{J}$ is useful for finding likely reconnection events in large data sets (e.g., Cluster and MMS)

Correspondence to:
M. Hamrin,
hamrin@space.umu.se

Citation:
Hamrin, M., L. Andersson, A. Vaivads, T. Pitkänen, and H. Gunell (2015), The use of the power density for identifying reconnection regions, *J. Geophys. Res. Space Physics*, *120*, 8644–8662, doi:10.1002/2015JA021535.

Received 3 JUN 2015
Accepted 23 SEP 2015
Accepted article online 30 SEP 2015
Published online 26 OCT 2015

©2015. American Geophysical Union. All Rights Reserved.

The use of the power density for identifying reconnection regions

M. Hamrin[1], L. Andersson[2], A. Vaivads[3], T. Pitkänen[1], and H. Gunell[4]

[1]Department of Physics, Umeå University, Umeå, Sweden, [2]LASP, Boulder, Colorado, USA, [3]Swedish Institute of Space Physics, Uppsala, Sweden, [4]Belgian Institute for Space Aeronomy, Brussels, Belgium

Abstract In the vicinity of magnetic reconnection, magnetic energy is transferred into kinetic energy. A reconnection region hence corresponds to a load, and it should manifest itself as large and positive values of the power density, $\mathbf{E} \cdot \mathbf{J} \gg 0$, where $\mathbf{E}$ is the electric field and $\mathbf{J}$ the current density. In this article we analyze Cluster plasma sheet data from 2001–2004 to investigate the use of the power density for identifying possible magnetic reconnection events from large sets of observed data. From theoretical arguments we show that an event with $\mathbf{E} \cdot \mathbf{J} \gtrsim$20 pW/m^3 in the Earth's magnetotail observed by the Cluster instruments ($X < -10R_E$ and $|Y| \lesssim 10R_E$) is likely to be associated with reconnection. The power density can be used as a primary indicator of potential reconnection regions, but selected events must be reviewed separately to confirm any possible reconnection signatures by looking for other signatures such as Hall electric and magnetic fields and reconnection jets. The power density can be computed from multispacecraft data, and we argue that the power density can be used as a tool for identifying possible reconnection events from large sets of data, e.g., from the Cluster and the Magnetospheric Multiscale missions.

1. Introduction

Magnetic reconnection is a process where magnetic energy is converted into particle energy and where the magnetic field topology is changed. Reconnection is a fundamental process in many astrophysical plasmas. For example, it is important for the formation of solar flares [*Giovanelli*, 1946]. Reconnection is also a key process for the energy transfer into and within the Earth's magnetosphere [*Dungey*, 1961] as well as at other solar system objects since it controls both the transfer of energy across the magnetopause and the release of stored energy in the magnetotail as fast plasma flows [*Paschmann et al.*, 1979].

The Earth's magnetosphere is an easily accessible natural laboratory for studying magnetic reconnection, and data from several magnetospheric missions are available for investigations. However, it is often a complicated and time-consuming task to find suitable reconnection events to analyze from the enormous amount of data from missions such as Cluster and Magnetospheric Multiscale (MMS). The selection process often involves visual inspection and analysis of large data sets. An automatic method, which can be used for selecting potentially interesting reconnection events, would of course be very useful since it could reduce the amount of data that need to be processed manually.

A few lists of known Cluster reconnection events are reported in the literature, e.g., *Østgaard et al.* [2009], *Eastwood et al.* [2010], and *Borg et al.* [2012]. *Eastwood et al.* [2010] searched by visual inspection for reconnection signs in the Cluster C1 and C3 data from the first five tail seasons, 2001–2005. A total of 33 events were selected, all showing significant and correlated V_x and B_z reversals as expected for reconnection encounters. *Østgaard et al.* [2009] investigated 13 Cluster reconnection encounters from 2001–2004, most of which overlap partly or entirely with the events from *Eastwood et al.* [2010]. Six of the events from *Østgaard et al.* [2009] had available auroral imaging data to compare with. *Borg et al.* [2012] studied the ion diffusion region of 21 Cluster reconnection encounters in the magnetotail from 2001–2006. The events were selected by manual inspection. The list also includes events from *Eastwood et al.* [2010], and it is a continuation of the events reported in *Borg* [2006]. Many of the events documented in *Østgaard et al.* [2009], *Eastwood et al.* [2010], and *Borg et al.* [2012] have also been addressed in other investigations [e.g., *Baker et al.*, 2002; *Runov et al.*, 2003; *Eriksson et al.*, 2004; *Borg et al.*, 2005; *Cattell et al.*, 2005; *Wygant et al.*, 2005; *Wei et al.*, 2007; *Chen et al.*, 2008; *Retino et al.*, 2008; *Snekvik et al.*, 2012; *Fu et al.*, 2013]. Besides the three mentioned Cluster magnetotail

reconnection event lists above, there are only a few additional Cluster events reported in the literature. For example, *Nakamura et al.* [2002] investigated a fast flow event from 12 August 2001, at ~18:40 UT. It was found to be associated with a small auroral substorm, and it was suggested to be located near a reconnection region. *Eastwood et al.* [2005] investigated two reconnection sites surrounding an Earthward moving flux rope at 2 October 2003, ~00:47 UT.

In the present article, we will discuss the importance of the power density $\mathbf{E} \cdot \mathbf{J}$, where $\mathbf{E}$ is the electric field and $\mathbf{J}$ is the current density, for identifying possible reconnection events from large sets of data. The power density measures the amount of energy (per unit time and volume) that is converted between electromagnetic and kinetic energy. Energy is transferred from the particles to the fields, and the electromagnetic energy density increases locally when $\mathbf{E} \cdot \mathbf{J} < 0$ (if the Poynting flux can be neglected). This can be considered a generator (dynamo) process. Energy is transferred in the opposite direction from the fields to the particles when $\mathbf{E} \cdot \mathbf{J} > 0$ (load process), and the electromagnetic energy density decreases. Multispacecraft missions such as Cluster [*Escoubet et al.*, 1997] are favorable for observational investigations of energy conversion using $\mathbf{E} \cdot \mathbf{J}$. The reason is that at least four simultaneous magnetic field measurements are needed for estimating $\mathbf{J}$ with the curlometer method ($\mathbf{J} \approx \nabla \times \mathbf{B}/\mu_0$).

The power density has proven to be very useful when analyzing how energy is transferred between the fields and the particles. *Hamrin et al.* [2006] used Cluster observations of $\mathbf{E} \cdot \mathbf{J}$ to identify generator regions in the magnetotail and to relate them to auroral acceleration observed at lower altitudes by conjugated FAST data. Subsequently, the power density has been valuable for identifying both generator and load regions from Cluster observations in the plasma sheet [e.g., *Hamrin et al.*, 2011], and it has also been utilized to investigate the evolution of flux pileup regions in the plasma sheet and the possible braking of Earthward propagating flow bursts from observed Cluster data [*Hamrin et al.*, 2013, 2014]. The power density has also proven to be useful for investigating energy conversion in other regions of the magnetosphere, such as at the magnetopause. For example, *Rosenqvist et al.* [2006, 2008a] and *Anekallu et al.* [2011] integrated $(\mathbf{J} \times \mathbf{B}) \cdot \mathbf{v}$ ($= \mathbf{E} \cdot \mathbf{J}$ in ideal MHD) over magnetopause crossings using Cluster data and they estimated the local energy conversion.

In the process of magnetic reconnection, magnetic energy is transformed into particle energy in the form of bulk acceleration and heating in the vicinity of an *X* line [see, e.g., *Lapenta et al.*, 2014]. Reconnection can hence be considered as a load, and it should manifest itself as a region with $\mathbf{E} \cdot \mathbf{J} > 0$. The load nature of the *X* line region has been investigated numerically previously. For example, *Sitnov and Swisdak* [2011] used a full particle code to study the onset of reconnection in 2-D current sheets. In their Figure 4 they show that the ion energization, $\mathbf{E} \cdot \mathbf{J_i} > 0$, is localized in the vicinity of the *X* line within a region with a cross-tail width of a few ion inertial lengths c/ω_i and stretching several tens of c/ω_i along the magnetotail. The electron energization, $\mathbf{E} \cdot \mathbf{J_e} > 0$, on the other hand, is more localized in space and covers a smaller spatial region. A similar result was also obtained by *Lapenta et al.* [2014], who used a 3-D kinetic simulation to investigate the energy conversion downstream of a reconnection site. Their Figure 6 shows that the reconnection load can be observed quite far away from the tail but that the cross-tail dimension is rather narrow and of the order of a few c/ω_i. *Birn and Hesse* [2005] used a large-scale resistive MHD simulation to study the conversion and release of energy due to magnetotail reconnection. From their Figure 5a we see that clear regions of $\mathbf{E} \cdot \mathbf{J} > 0$ appear in separatrix-like regions, covering down-tail regions of several tens of R_E. It is worthwhile to note that the reconnection load region clearly appears within such an MHD simulation like the one discussed in *Birn and Hesse* [2005], even though the simulation does not include kinetic effects. This suggests that the multispacecraft Cluster instruments also should be able to detect and at least partly resolve the reconnection load region, even though the interspacecraft distances are of the order of ion scales.

In this article we will show that Cluster $\mathbf{E} \cdot \mathbf{J}$ data indeed can be used for investigating the reconnection load region. We will argue that the ion acceleration process near a reconnection region, and the corresponding energy conversion, can be analyzed through the power density observed by Cluster. We will use $\mathbf{E} \cdot \mathbf{J}$ basically as a qualitative (not quantitative) estimate of the energy conversion at ion scales as measured by the Cluster instruments. However, we do not claim that we can measure the exact magnitude of $\mathbf{E} \cdot \mathbf{J}$ very exactly since it depends on, e.g., the scale size of the measurements and higher-resolution data generally resolve smaller-scale signature. Instead, we claim that a large and positive value of $\mathbf{E} \cdot \mathbf{J}$ is likely to be associated with reconnection. For the Cluster instrumentation, we will show that a threshold of $\mathbf{E} \cdot \mathbf{J}$ of ~20 pW/m^3 is suitable for the Cluster instrumentation for indicating possible reconnection events in the magnetotail. The new Magnetospheric Multiscale (MMS) mission is designed to study the microphysics of,

e.g., reconnection at spacecraft distances smaller than for Cluster. It is likely that $\mathbf{E} \cdot \mathbf{J}$ obtained from MMS also will prove to be very useful for analyzing the smaller-scale physics and that it can be used as a "reconnection parameter" to quickly select potentially interesting reconnection events from the steadily increasing amount of data.

The article is organized as follows. In section 2 we give a simple theoretical motivation for the use of the power density for probing the reconnection load region, and we estimate a threshold value of $\mathbf{E} \cdot \mathbf{J}$ to be used when searching for potential reconnection events. In section 3 we briefly discuss the data used. In the next two sections we present the observations, starting out with two sample events in section 4 and a statistical investigation in section 5. Our results are discussed and summarized in section 6.

2. Theoretical Motivation

In this section we derive an approximate reconnection threshold value for $\mathbf{E} \cdot \mathbf{J}$ by using a simple model of reconnection. The frozen-in condition is fulfilled outside the reconnection diffusion region. The plasma and the magnetic field lines convect toward the region with the $\mathbf{E} \times \mathbf{B}$ velocity which typically is $\sim 0.1 V_A$, where V_A is the upstream Alfvén velocity. After acceleration in the potential well, ions exit the reconnection region as high-speed jets with velocities $\sim 1 V_A$ [*Petschek*, 1964; *Yamada et al.*, 2010]. A typical value of the corresponding $\mathbf{E} \cdot \mathbf{J}$ of this reconnection load can be obtained in this simple picture.

The tangential reconnection electric field can be estimated in the inflow region as $E = |-\mathbf{V} \times \mathbf{B}| \sim 0.1 V_A B_L$, where B_L ~20 nT is the typical lobe magnetic field. Assuming a proton plasma with density 0.3 cm^{-3}, the Alfvén velocity is $V_A = B_L/\sqrt{(\mu_0 n m_p)} \sim 800$ km/s and $E \sim 0.1 V_a B_L$ ~2 mV/m. As can be seen from Figure 14 in *Wygant et al.* [2005], the tangential electric field corresponds to nearly vertical equipotential contours in the inflow region far from the current sheets (separatrices). However, closer to the bifurcated current sheet, the equipotentials are horizontally deflected consistent with the normal electric field responsible for the ion acceleration.

Similar potential structures have been measured in laboratory experiments by *Egedal et al.* [2011], who showed that a current system is set up in the reconnection region, where ion polarization currents perpendicular to $\mathbf{B}$ are closed by parallel currents carried by electrons close to the X line. Investigating the physics behind these potentials, *Egedal et al.* [2008] showed that a combination of magnetic and electric trapping of electrons can explain the formation of the potential structures and that these are responsible for the anisotropic electron pressure that has been observed in reconnection regions both in the magnetotail and in laboratory experiments.

The current density of the bifurcated current sheet can be estimated from Ampères law according to $J \approx |\nabla \times \mathbf{B}|/\mu_0 \sim B_L/(\mu_0 L)$ where L is the typical thickness of the reconnection region. L depends on the distance from the X line. From numerical simulations it can be seen that L is of the order 1 or a few hydrogen ion inertial lengths [e.g., *Daughton et al.*, 2006, 2009; *Sitnov and Swisdak*, 2011; *Lapenta et al.*, 2014]. Assuming a scale length of about three ion inertial lengths, we obtain $L \sim 3c/\omega_{H+}$ ~1200 km for a plasma with density 0.3 cm^{-3} and therefore $J \sim B_L/(\mu_0 L)$ ~10 nA/m^2.

Using these approximate values of E ~2 mV/m and J ~10 nA/m^2, we find that the reconnection load corresponds to $\mathbf{E} \cdot \mathbf{J}$ ~20 pW/m^3. This is clearly larger than the typical (median or mean) load peak value of the power density observed by Cluster within the plasma sheet [see *Hamrin et al.*, 2009, Figure 5, panel 2]. In this article, we will use 20 pW/m^3 as a threshold that indicates that an event is likely to be associated with reconnection in Earth's magnetotail.

3. Instrumentation and Data

In this article we use plasma sheet data from 2001–2004 from the Electric Field and Wave (EFW) experiment, the Cluster Ion Spectroscopy (CIS) experiment, and the Fluxgate Magnetometer (FGM) instrument on board the four-spacecraft Cluster mission [see *Escoubet et al.*, 2001, and references therein]. All data have been downloaded from the Cluster Science Archive (CSA) (http://www.cosmos.esa.int/web/csa).

We will utilize multispacecraft methods to compute $\mathbf{E} \cdot \mathbf{J}$: The curlometer will be used for estimating the current density, and the electric field will be averaged over available instruments. However, we will compare the multispacecraft curlometer current with a single-satellite estimate, and the electric field observations from different instruments will be compared to verify the reliability of our $\mathbf{E} \cdot \mathbf{J}$ estimate.

Table 1. Cluster Tetrahedral Configuration in the Plasma Sheet

Year	Approximate Scale Size (km)
2001	1500
2002	3000
2003	200
2004	1000
2005 and onward	Multiscale mode

The full current density can be obtained by the multispacecraft curlometer method, $\mathbf{J} \approx \nabla \times \mathbf{B}/\mu_0$, by using magnetic field data from the FGM instrument on board all four spacecraft [*Paschmann and Schwartz*, 2000; *Dunlop et al.*, 2002]. The quantity $|\nabla \cdot \mathbf{B}|/|\nabla \times \mathbf{B}|$ can be used as a qualitative error estimate for the curlometer current [*Paschmann and Schwartz*, 2000], but a one-to-one correspondence to the true error is not expected. In theory, $|\nabla \cdot \mathbf{B}|/|\nabla \times \mathbf{B}| = 0$ but in practice the estimate of it can vary substantially, for example, due to neglected nonlinear spatial gradients. An often used upper limit of $|\boldsymbol{\nabla} \cdot B/\boldsymbol{\nabla} \times \mathbf{B}|$ is ~50% [*Paschmann and Schwartz*, 2000; *Dunlop et al.*, 2002]. The curlometer estimate depends on the size and shape of the Cluster tetrahedron. Current density structures much smaller than the tetrahedron cannot generally be resolved, and the estimate is usually better if the tetrahedron is approximately equilateral in shape, i.e., the elongation and the planarity of the tetrahedron is small. The characteristic size of the tetrahedron evolved over the years (see Table 1). This implies that the current density will be resolved on different scales for different years. The highest spatial resolution of the curlometer current is obtained in 2003 when the Cluster scale size was of the order of an ion inertial length c/ω_{H+} ($c/\omega_{H+} \sim 400$ km using typical values of 0.3 cm^{-3} and 20 nT). In 2005 and later years, the satellites were in a multiscale mode, implying that the configuration was not suitable for computing the current density.

The curlometer method is generally believed to produce best results when compared to the single-satellite method, and it realistically determines the current density even for cases where the scale size of the Cluster tetrahedron is of the order of the current layer thickness [*Dunlop and Eastwood*, 2008]. *Rosenqvist et al.* [2008b] and *Anekallu et al.* [2011] found that the single-spacecraft current sometimes yields a different sign for the energy conversion than when using the curlometer current. They argued that this discrepancy can be caused by large normal current contributions and/or a time offset between the **E** and **J** data used for the power density. In this article we avoid time offsets by using the electric field averaged over the spacecraft together with the curlometer current, which can be interpreted as an average value over the Cluster tetrahedron. Moreover, we only use data from the Cluster tail seasons where the spacecraft are approximately homogeneously distributed in space, i.e., the Cluster tetrahedron is nearly equilateral, and the elongation and the planarity are small. *Rosenqvist et al.* [2008b] and *Anekallu et al.* [2011], on the other hand, used data from dayside and flank magnetopause crossings where the Cluster tetrahedron is less uniform.

The electric field can be measured directly by the EFW instrument by using probes on wire booms in the satellite's spin plane. The full electric field vector is estimated from the assumption $\mathbf{E} \cdot \mathbf{B} = 0$. Any possible effects from parallel electric fields are hence neglected in our study. Even though EFW is operational on all spacecraft, the full electric field vector is not always available. This is often due to a close alignment of the **B** vector with the spacecraft's spin plane (the assumption $\mathbf{E} \cdot \mathbf{B} = 0$), and it is a common cause for EFW data gaps in the plasma sheet. Assuming that the magnetic field is approximately frozen in the plasma, the (perpendicular) electric field can also be estimated from ion velocity moments from the CIS Composition and Distribution Function (CODIF) analyser and the CIS Hot Ion Analyzer (HIA) according to $\mathbf{E} \sim -\mathbf{V} \times \mathbf{B}$. From CODIF we use the moments for H^+ ions; however, HIA does not have mass separation. HIA is operational on spacecraft C1 and C3, while CODIF is operational on C1, C3, and C4 but suffers from a higher noise level on C3, especially during later years. Neither EFW nor CIS can measure electric fields parallel to the magnetic field, and effects from parallel fields on $\mathbf{E} \cdot \mathbf{J}$ are neglected in our investigation. *Egedal et al.* [2009] used kinetic simulations of guide-field reconnection to show that the parallel electric field is localized in space and that its structure does not significantly energize the electrons even though it is important for the trapping of electrons and it influences reconnection rates [*Egedal et al.*, 2013]. Parallel electric fields should be a topic for future research when multipoint three-dimensional electric field data from the MMS spacecraft become available [*Burch et al.*, 2015].

In this article we show that direct electric field measurements from EFW, as well as electric field estimates from the CIS ion moments, can be used for obtaining an approximate value of $\mathbf{E} \cdot \mathbf{J}$, even though the frozen-in condition is not formally valid close to reconnection and CIS usually underestimates the electric field. For the average electric field used together with the curlometer current in $\mathbf{E} \cdot \mathbf{J}$ we compute one CIS estimate and one EFW estimate by averaging over all operating CIS (CODIF and HIA) or EFW instruments on board the satellites. The spatial resolution of $\mathbf{E} \cdot \mathbf{J}$ consequently varies over the years according the Cluster tetrahedron scale size as presented in Table 1. It resolves the smallest structures in 2003 and largest structures in 2002.

Unless otherwise stated, we use the GSM coordinate system. However, the DSI system (Despun System Inverted) is particularly useful when comparing the electric field E_x and E_y obtained from the EFW and CIS instruments. This is because DSI is the inherent spacecraft system with the EFW probes in the DSIxy plane. DSI is closely aligned with GSE (it differs only with a few degrees) but differs from GSM with some tens of degrees in the plasma sheet probed by Cluster.

We compute $\mathbf{E} \cdot \mathbf{J}$ in a frame stationary with respect to the Earth (e.g., GSM or DSI). However, one could also argue that it should be computed in the frame of the X line which is possibly moving. This may influence the result since the electric field is not invariant under nonrelativistic coordinate transformations. *Wygant et al.* [2005] discussed the effect of observing the electric field in a frame moving relative to the X line. They conducted a statistical analysis of about 30 individual and nearby current sheet crossings in the vicinity of a reconnection region, and they observed a small DC offset in the average electric field (in the normal direction). *Wygant et al.* [2005] argued that one possible cause for this small DC offset could be a convective electric field due to the motion of the frame of reference relative to the X line.

To further analyze the effect of a relative motion of the chosen frame of reference, and a possible DC offset in the electric field observations, we have reviewed documented reconnection events in *Eastwood et al.* [2010]. By investigating how the magnetic field signatures pass over the Cluster satellites, we find that the typical speed of an X line is 50–100 km/s (Earthward or tailward) during these events. This velocity estimate is consistent with what was obtained by *Baker et al.* [2002], who discussed an observation from 27 August 2001 and who found that the X line moved tailward with ∼100 km/s. Assuming $V \lesssim 100$ km/s and $|B| \lesssim 10$ nT (documented reconnection regions in, e.g., *Eastwood et al.* [2010] are often identified using observations quite close to the neutral sheet, i.e., $|B|$ is quite small), we find that a transfer of coordinates to a frame which is at rest with respect to the X line corresponds to a correction in the electric field corresponding to $|\Delta E| \lesssim 1$ mV/m. This is in most cases significantly smaller than the observed electric field in the vicinity of reconnection (also as observed by CIS), and it will therefore be neglected in our investigation.

4. Observations

4.1. The 1 October 2001 Event

To demonstrate the use of the power density for localizing possible reconnection events, we first start by discussing Cluster data from 1 October 2001, when the spacecraft showed multiple encounters with a reconnection region. The data have previously also been investigated in detail by *Runov et al.* [2003] and by *Wygant et al.* [2005].

Runov et al. [2003] investigated the time interval 09:47–09:51 UT when Cluster crossed the magnetotail neutral sheet four times. They studied the high-speed proton flow reversals and magnetic field variations and concluded that a tailward moving X line passed over the spacecraft. Quadrupolar magnetic Hall field signatures were used to confirm that an X line was detected. Figure 4 of *Runov et al.* [2003] schematically shows how Cluster probes different regions near the X line due to magnetotail flappings.

Wygant et al. [2005] conducted a detailed investigation of one single current sheet crossing at ∼09:46:50 UT, as well as a statistical investigation of about 30 nearby current sheet crossings during the interval 09:40–09:55 UT. The ion acceleration was discussed in detail by *Wygant et al.* [2005]. They showed that individual ions are ballistically accelerated by a potential drop across a bifurcated current sheet. Protons are accelerated within a region of 60–100 km by a 4–6 kV potential structure caused by electric fields normal to the current sheet. O^+ ions, on the other hand, are accelerated by a potential drop of 10–30 kV within a larger-scale-size potential structure (1000–3000 km) associated with a larger-scale current sheet.

In the upstream region, *Wygant et al.* [2005] showed that protons $\mathbf{E} \times \mathbf{B}$ drift through the larger-scale structure until they reach the smaller-scale potential structure closer to the X line. In such small-scale regions of the

order of the proton gyroradius, the protons become unmagnetized. In the single-particle picture the proton ions are accelerated ballistically by the potential drop. O^+ ions with their 16 times larger gyroradius become unmagnetized already within the larger-scale potential structure. Electrons, on the other hand, $\mathbf{E} \times \mathbf{B}$ drift through both structures, hereby possibly contributing substantially to the electric current density within the bifurcated current sheet structure [*Wygant et al.*, 2005].

The accelerated ions form two counterstreaming beams inside the potential well [see *Wygant et al.*, 2005, Figure 5]. After the ballistic acceleration of the ions, the counterstreaming ion motion must be converted into reconnection exhaust jets in the outflow directions. There are many possible mechanisms. *Wygant et al.* [2005], for example, discuss the specular ion reflection off the electrostatic walls within the diverging geometry of the bifurcated current sheet. However, other scenarios are also mentioned, e.g., acceleration by an electric field component along the exhaust direction and the Speiser mechanism [*Speiser*, 1965]. In the fluid picture, the incident $\mathbf{E} \times \mathbf{B}$ ion flow appears to be converted into a high-speed bulk flow or jet [*Petschek*, 1964].

Using magnetic minimum variance analysis on the current sheet crossings, *Wygant et al.* [2005] computed the normal vector of the current sheets and they found that it could vary substantially between the events. Some crossings had a normal approximately aligned with GSE*z*, while others could have normals with significant GSE*y* components. The current sheet at ~09:46:50 was strongly tilted from the equatorial plane, and the normal (−0.05, 0.80, −0.59) had a substantial GSE*y* component possible due to kink mode waves propagating duskward in the magnetotail. Such kink-like waves are suggested to be the cause for magnetotail north-south flappings, and they give rise to a vertical motion with velocities of 50–100 km/s [e.g., *Sergeev et al.*, 2006; *Volwerk et al.*, 2013; *Kubyshkina et al.*, 2014].

The tilt of the current sheet at ~09:46:50 implies that the normal component of the electric field mainly is in GSE*y*, i.e., $E_{\mathrm{norm}} \sim E_y$ for this current sheet crossing. E_{norm} is the electric field component responsible for the ion acceleration across the separatrix regions [see *Wygant et al.*, 2005, Figure 5], and it should point toward the current sheet. Similarly, the reconnection electric field which causes the $\mathbf{E} \times \mathbf{B}$ drift of the plasma into the reconnection region should be along GSE*z* for this event, i.e., $E_{\mathrm{tan}} \sim E_z$.

An overview of the multiple current sheet crossings on 1 October 2001 can be found in Figure 1. The time interval containing the ~09:46:50 current sheet crossing is highlighted in yellow. Figures 1a–1f show the magnetic field and plasma flow velocity components in the GSE system. The multiple crossings can be observed as the rapid changes in the sign of B_x as seen from Figure 1a. Figure 1g shows the power density $\mathbf{E} \cdot \mathbf{J}$ obtained by multiplying the curlometer current density with the average electric field from EFW (red) and CIS (black). The dashed horizontal lines indicate the levels 20 pW/m^3 and 30 pW/m^3, respectively. As discussed in section 2, we expect that $\mathbf{E} \cdot \mathbf{J} \gtrsim 20$ pW/m^3 near an *X* line. From Figure 1 we indeed see that the CIS estimate of $\mathbf{E} \cdot \mathbf{J}$ many times exceeds both the 20 pW/m^3 and 30 pW/m^3 levels. The same is true for the EFW estimate whenever data are available.

The fact that the power density is positive indicates that this is a region dominated by load processes, possibly a consequence of the ion acceleration near the *X* line. *Wygant et al.* [2005] discussed in detail the acceleration of ions by E_{norm} for the event at ~09:46:50. From Figure 1 we see that the ion acceleration region discussed by *Wygant et al.* [2005] coincides with a region with $\mathbf{E} \cdot \mathbf{J} \gg 0$. It is hence likely that $\mathbf{E} \cdot \mathbf{J}$ captures the energy conversion corresponding to this ion acceleration.

Spacecraft C4 was found to cross the reconnection region within one H^+ inertia length c/ω_{H+} of the *X* line during the event presented in *Wygant et al.* [2005]. Spacecraft C1, on the other hand, crossed further downstream at about $3c/\omega_{H+}$. Even though the main focus was on physical processes at the subion inertial length scale in the neighborhood of the current sheet crossing at 09:46:47, it is worthwhile to note that *Wygant et al.* [2005] still observed clear signatures of ion acceleration, even when using lower resolution 4 s velocity moment data from the ion instruments.

Figure 2 presents current density data obtained with two different methods: the curlometer method and the single-satellite method, $J \approx \Delta B_x/(\mu_0 V \Delta t)$, where *V* describes the relative velocity of the spacecraft as they cross the current sheet along the current sheet normal. Only data from the main current sheet crossing (09:46:45–09:47:45 UT) are presented. High-resolution (five vectors per second) magnetic field data are used for the single-satellite current estimates. For the curlometer current, however, we have only used low-resolution (4 s) magnetic field data since the current density will subsequently be multiplied with 4 s resolution electric field data to obtain $\mathbf{E} \cdot \mathbf{J}$. Using B_x timing analysis between the spacecraft, we find that the

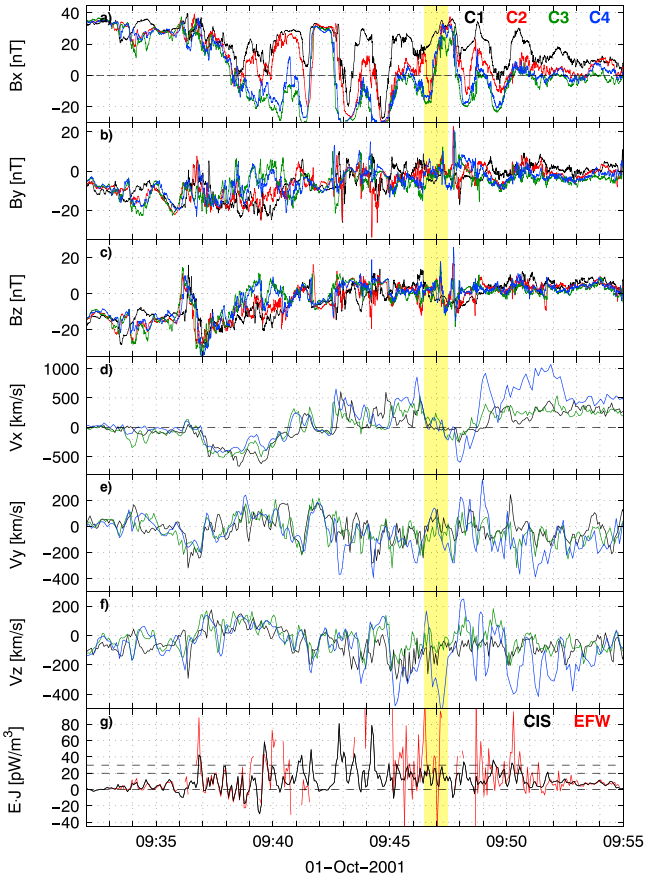

Figure 1. Overview of the event from *Wygant et al.* [2005] (highlighted in yellow). (a–c) FGM magnetic field observed by the four Cluster spacecraft. (d–f) Plasma flow velocity obtained by CIS-HIA on C1 and C3 and obtained by CIS-CODIF on C4. (g) Power density computed from the curlometer current and the average electric field from the CIS (black) and EFW instruments (red), respectively. The horizontal lines indicate the levels 20 pW/m^3 and 30 pW/m^3. The data are presented in the GSE system.

velocity of the current sheet relative to the spacecraft is $\mathbf{V} = (-0.10, 85, -36)$ km/s. This is consistent with the result of *Wygant et al.* [2005], who found that the current sheet velocity was 60–100 km/s. It is also consistent with the current sheet normal as can be shown from minimum variance analysis applied on the magnetic B_x component [*Wygant et al.*, 2005]. The current sheet will hence mainly be oriented in the GSE*yz* plane.

Figure 2a shows the components of the curlometer current in the GSE system. The single-satellite estimate of the cross-tail current obtained from all four spacecraft are presented in Figure 2b. As can be seen from Figure 1a, there are higher frequency disturbances in the main B_x signature of the current sheet crossing. These disturbances can be caused by, e.g., wave motions and deviations from $V \approx$ constant. Since we want to estimate the current density of the primary current sheet, J_{cs}, we have smoothed the current density with an 8 s running average. However, some fluctuations are still present in the resulting J_{cs} in Figure 2b, even causing a few samples with $J_{cs} < 0$ (which implies that there has been a negative slope in the B_x curve).

Figure 2c shows the single-satellite current averaged over the Cluster spacecraft (black) and the magnitude of the curlometer current (red), which also could be considered as an average over the Cluster tetrahedron. We see that there is a good agreement between the single-satellite and the curlometer current. In Figure 2d we show $|\nabla \cdot \mathbf{B}|/|\nabla \times \mathbf{B}|$, which can be used as an indication of the quality of the curlometer estimate. We see that $|\nabla \cdot \mathbf{B}|/|\nabla \times \mathbf{B}|$ is clearly smaller than 50% during the current sheet crossing, and the curlometer is expected to work satisfactory. Moreover, the Cluster tetrahedron is approximately equilateral (elongation $\approx$ 0.09 and planarity $\approx$ 0.08), which is optimal for the curlometer method. Note also that *Runov et al.* [2003] conducted investigations of the applicability of the multispacecraft method for estimating the current density. They found that the correlation between the magnetic field measurements from the four spacecraft was high.

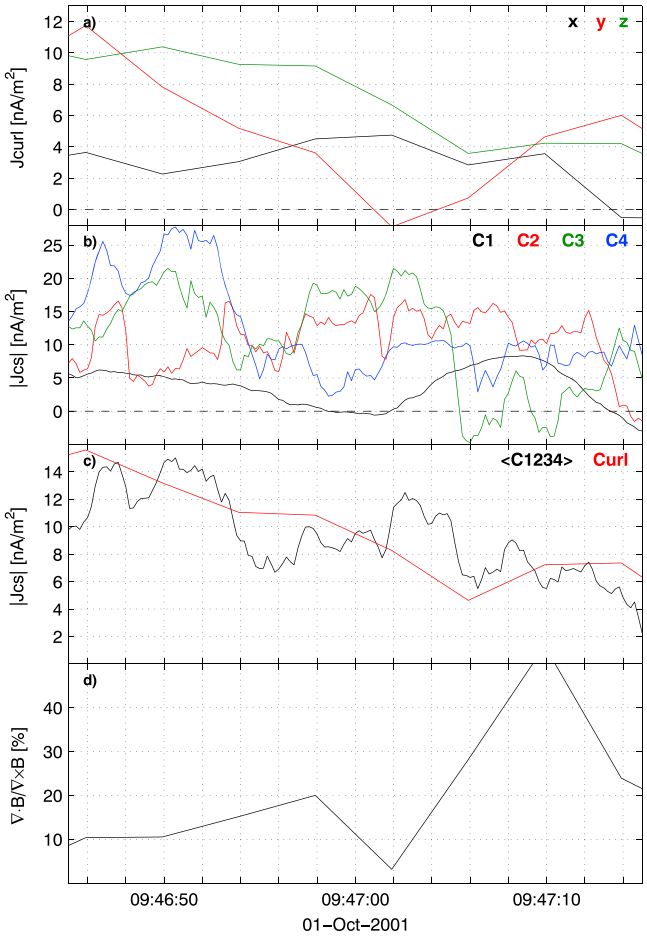

Figure 2. Current density for the main current sheet crossing of the *Wygant et al.* [2005] event. (a) Curlometer current density components in GSE. (b) Cross-tail current sheet density obtained with the single-satellite method from B_x data measured on all four Cluster spacecraft. (c) Single-satellite current averaged over the four spacecraft (black) and magnitude of the curlometer current (red). (d) A quality estimate, $|\nabla \cdot \mathbf{B}|/|\nabla \times \mathbf{B}|$, of the curlometer current.

The spacecraft therefore probed the same physical region, and a technique such as the curlometer should be appropriate to use for estimating the current density. We hence conclude that the curlometer should be reliable during this event.

In Figure 3 we present the electric field observed by the Cluster spacecraft C1, C3, and C4. The field is expressed in the DSI coordinate system with DSI*x* and DSI*y* oriented in the satellites' spin plane, i.e., in the plane containing the EFW probes. The gray curves show the full-resolution EFW electric field, while the red lines correspond to the spin-averaged field downloaded from CSA. The blue and cyan lines show the electric field derived from the CODIF and HIA ion moments according to $-\mathbf{V} \times \mathbf{B}$. From Figure 3 we see that the spin-averaged EFW estimate (red) naturally smooths the full-resolution (gray) electric field. The CIS estimates (blue and cyan) underestimate the electric field even more (except for C1), but it still captures the general variation. The CIS estimate is based on the assumption that the ions are frozen into the magnetic field. This assumption is not formally valid in the reconnection diffusion region. However, it is remarkable that the CIS estimate (in particular CODIF) resolves the electric field variations so well, although it underestimates the magnitude of the electric field. Even though the magnitude of $\mathbf{E} \cdot \mathbf{J}$ will be underestimated, we find that the resulting value will not change sign when using CIS data instead of EFW data for the electric field. Qualitatively, $\mathbf{E} \cdot \mathbf{J}$ will still be large and positive ($\gtrsim$ 20 pW/m^3), and we therefore argue that it can be estimated by using only the CIS electric field for this event.

Computing the correlation coefficient between the spin-averaged EFW electric field and the CIS estimate, we obtain moderate to strong correlation for the E_y component (the dominant component in the spin plane):

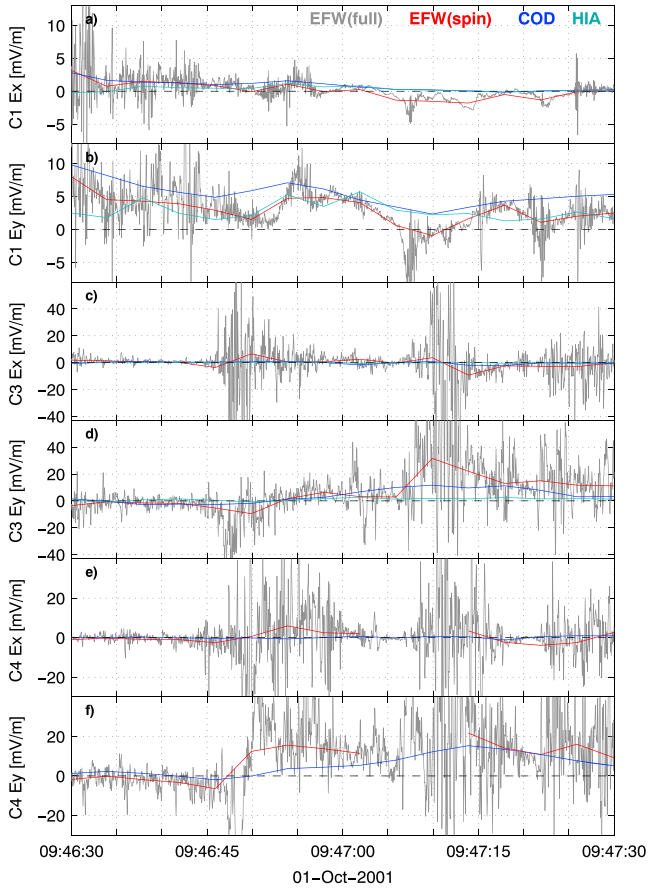

Figure 3. Electric field E_x and E_y components in the DSI system (in the satellite spin plane) for the *Wygant et al.* [2005] event. Data from C1, C3, and C4 are shown. The gray curves show the full-resolution EFW electric field, while the red curves correspond to the spin-averaged field downloaded from CSA. The blue and cyan curves show the CODIF and HIA estimates.

0.77, 0.79, and 0.74 for EFW-CODIF on C1, C3, and C4, and 0.44 and 0.59 for EFW-HIA on C1 and C3. The correlation coefficient is weaker for HIA, possibly caused by a high O^+ density during the event (not shown). The correlation coefficient for the E_x component is generally somewhat weaker. However, this is not unexpected since $|E_x|$ is considerably smaller than $|E_y|$. Moreover, E_x will not contribute significantly to $\mathbf{E} \cdot \mathbf{J}$ since the dominant current density components are J_y and J_z.

We have also computed the ratio between the DSI E_y components obtained from the spin-averaged EFW data and from the CIS ion moments, i.e., $E_y^{\mathrm{CIS}}/E_y^{\mathrm{EFW}}$. The ratio has only been computed in regions of strong electric fields, defined as E_y^{EFW} larger than one third of the peak value (the peak is defined as the 99.7 percentile). We find that the ratios are 1.53, 0.40, and 0.48 for CODIF-C1, C3, and C4, and 0.72 and 0.11 for HIA-C1 and C3. Hence, CIS typically underestimates the electric field (except for CODIF on C1) for this event.

4.2. The 22 August 2001 Event

Eastwood et al. [2007] investigated the Hall electric and magnetic field structure for a reconnection event observed by Cluster on 22 August 2001. In particular, they focused on the interval 09:40:00–09:52:00 UT, when the spacecraft observed a jet reversal associated with an earthward moving *X* line. An overview of the data are shown in Figure 4, where the *Eastwood et al.* [2007] event is highlighted in yellow. The event was favorable since measurements were available simultaneously on both sides of the current sheet. As can be seen from B_x in Figure 4a, C3 crossed the current sheet first and remained south of it before the other spacecraft crossed at later times. *Eastwood et al.* [2007] observed a quadrupole magnetic Hall field signature in the diffusion region. From the high-resolution EFW data they also observed strong (~40 mV/m) and symmetric Hall electric fields pointing toward the current sheet.

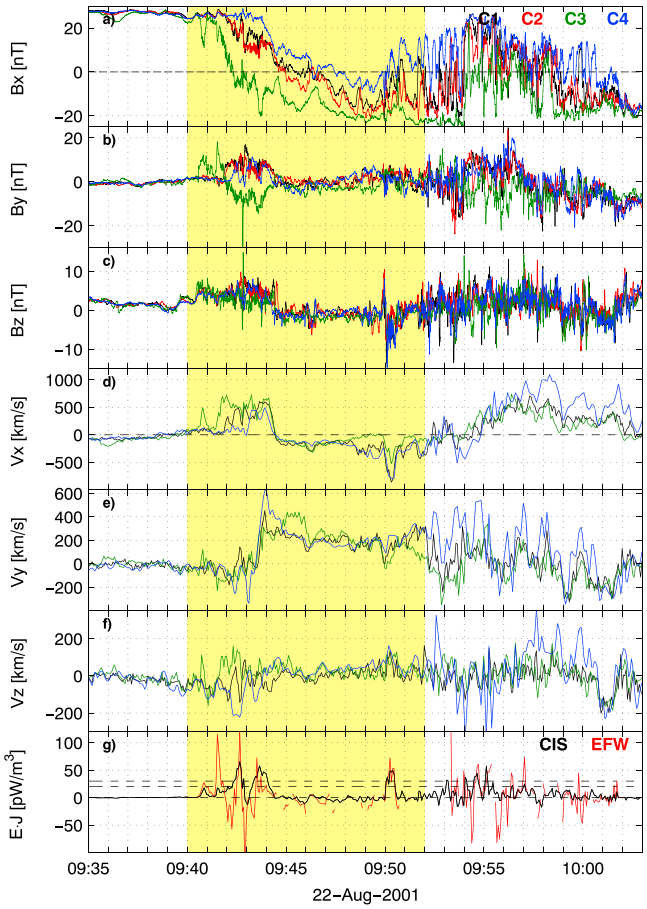

Figure 4. Overview of the *Eastwood et al.* [2007] event (highlighted in yellow). Same panels as in Figure 1, but the GSM system has been used.

From Figure 4g we see that the power density reaches high values during the *Eastwood et al.* [2007] event. $\mathbf{E} \cdot \mathbf{J}$ largely exceeds 30 mV/m for several samples (both when using EFW and CIS data for the electric field). Moreover, $\mathbf{E} \cdot \mathbf{J}$ also remains large for a while after the *Eastwood et al.* [2007] event: Between 09:52 and 09:58 we see high values of $\mathbf{E} \cdot \mathbf{J}$ together with another set of repeated jet reversals (tailward-earthward-tailward-earthward) and tail flappings. Preliminary investigations (not shown) indicate that the period 09:52–09:58 also is associated with reconnection.

Eastwood et al. [2007] argue that the curlometer is not optimal for estimating the structure of interest since the size of the current sheet is of the order of the size of the Cluster tetrahedron. Instead, they claim that the single-satellite method should be used. In Figure 5 we present the curlometer and single-satellite current density. Only data from the main current sheet crossing are shown, 09:40–09:49, i.e., the part of the *Eastwood et al.* [2007] event with largest power densities. Similar to the previous event, there are fluctuations in the B_x data, and the single-satellite current has therefore been smoothed by a 60 s running average. Using timing between the satellites, we find that the current sheet velocity is $(2.6, -3.2, 9.4)$ km/s which is consistent with the current sheet normal obtained from minimum variance analysis applied on B_x*Eastwood et al.* [2007]. From Figure 5c we see that the single-satellite method and the curlometer agree well (in both magnitude and signature). Moreover, $|\nabla \cdot \mathbf{B}|/|\nabla \times \mathbf{B}|$ is generally significantly smaller than 50%, and we conclude that the curlometer also works satisfactorily for this event.

In Figure 6 we show the electric field obtained from EFW and CIS on board C1, C3, and C4. Again, we see that the CIS estimate (both CODIF and HIA) captures the general trend of the electric field, even though CIS underestimates the magnitude, especially in the regions of the strongest fields (in the region 09:40–09:45). (Note that the regularly spaced pulses seen in the electric field are anomalies caused by the WHISPER instrument.)

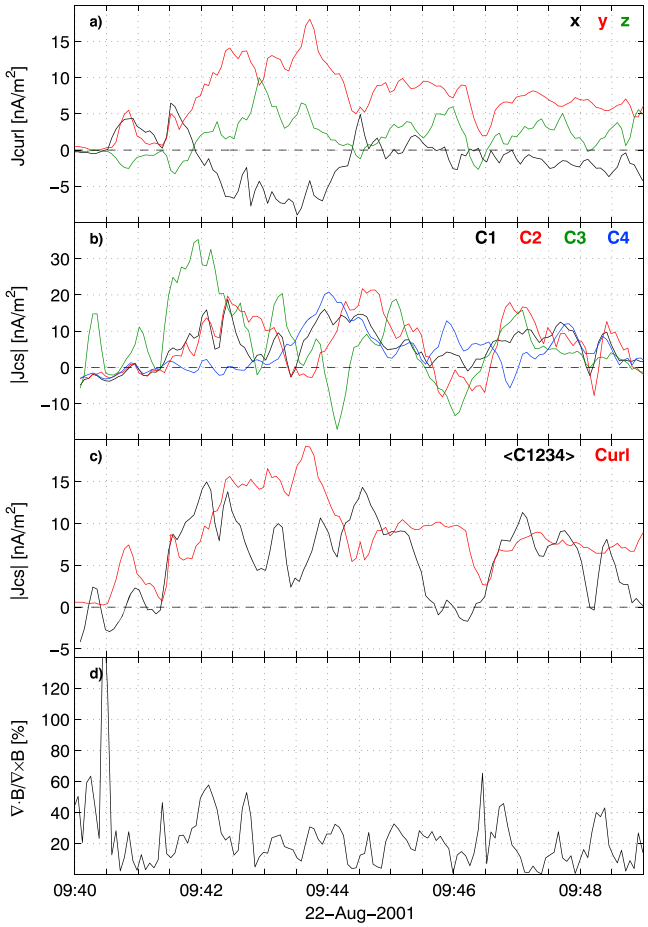

Figure 5. Current density for the main current sheet crossing of the *Eastwood et al.* [2007] event. Same panels as in Figure 2, but the GSM system has been used.

Correlation coefficients between the spin-averaged EFW E_y CIS estimate are 0.74, 0.81, and 0.77 for EFW-CODIF on C1, C3, and C4, and 0.76 and 0.52 for EFW-HIA on C1 and C3. We hence find that the correlation is strong during the event. Similar to the previous event, the correlation coefficient for the E_x component is weaker. However, the E_x is weak compared to E_y and does not contribute much to $\mathbf{E} \cdot \mathbf{J}$ since J_y is the dominant current density component.

Computing the ratio of E_y obtained from spin-averaged EFW and CIS ion moments (during strong fields), we find $E_y^{\mathrm{CIS}}/E_y^{\mathrm{EFW}}$ to be 0.40, 0.68, and 0.56 for CODIF-C1, C3, and C4, and 0.25 and 0.33 for HIA-C1 and C3. Hence, for this event CIS underestimates the electric field on the average ~0.4 (averaged over CODIF and HIA on C1, C3, and C4) when compared to the spin-averaged EFW E_y.

5. Statistical Investigations

5.1. Documented Reconnection Encounters

For a statistical investigation we have studied a set of Cluster reconnection encounters which are already documented in the literature. In particular, we have focused on the events discussed in *Østgaard et al.* [2009], *Eastwood et al.* [2010], and *Borg et al.* [2012]. However, we only include events from 2001–2004 when the Cluster configuration was optimal, even though a few events from 2005 also are discussed in the above references. Many of the events are included in all of these previous investigations, but the time extent of each event may vary between investigations. In Table 2 we have listed all the events, their start and stop times, their position in GSM coordinates, elongation, planarity, and which of the above investigations have previously discussed the events (E = *Eastwood et al.* [2010], B = *Borg et al.* [2012], and O = *Østgaard et al.* [2009]). In the case that an event has been included in more than one previous investigation, we have chosen to use the smallest

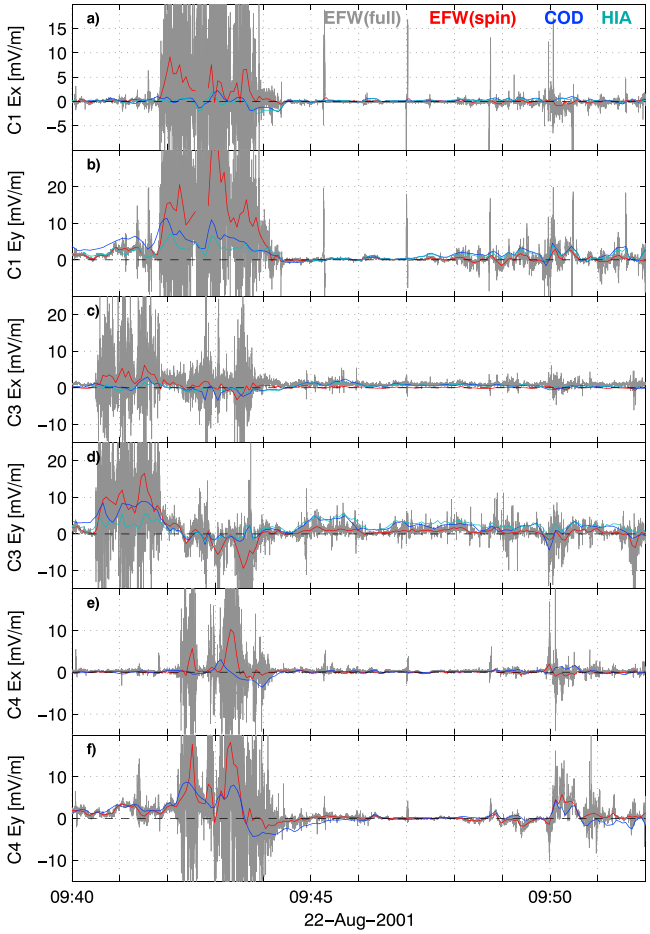

Figure 6. Electric field for the *Eastwood et al.* [2007] event in the DSI system. Same panels as in Figure 3.

T_1 and the largest T_2 for our investigation. For some of the events, note that we also may have changed the start and stop times somewhat, for example, to better include reconnection jet reversals.

From Table 2 we see that all events are observed for $-19 \leq X \leq -15\ R_E$ and $|Z| < 3.5\ R_E$. Except for event numbers 11 and 18, all events are also observed within $|Y| < 10\ R_E$.

The time extent of these events range from 4 min to ~1.5 h, with an average of 28 min. Note, however, that the time extent of the individual events may have been defined slightly differently in *Østgaard et al.* [2009], *Eastwood et al.* [2010], and *Borg et al.* [2012], but generally the events include dominant observed signatures of reconnection such as jet reversals, Hall fields, and diffusion regions. The Cluster spacecraft are in an approximately polar orbit, and near apogee the spacecraft move with a velocity of ~1 km/s. Even though the magnetotail often is flapping back and forth over the spacecraft (causing recurrent Cluster encounters with the same reconnection region), it is likely to expect that the average time extent of 28 min would roughly correspond to the time for Cluster to move through the main reconnection region along the orbit. Assuming that the cross-tail size of the main reconnection region is of the order of 5 ion inertial lengths of $c/\omega_{H+} \approx 400$ km for a 0.3 cm^{-3} plasma [e.g., *Daughton et al.*, 2006, 2009; *Sitnov and Swisdak*, 2011; *Lapenta et al.*, 2014], we note that the typical time extent of a Cluster reconnection encounter would be of the order ~30 min, which is consistent with the average time extent obtained from Table 2.

In Table 3 we present some relevant quantities for the 28 events listed in Table 2. Columns 2 and 3 contain the maximum value of $\mathbf{E} \cdot \mathbf{J}$ and the number of samples with $\mathbf{E} \cdot \mathbf{J}$ larger than the threshold of 20 pW/m^3 (see also section 2). The power density is computed using both the electric field derived from the CIS ion moments (averaged over CODIF and HIA on all spacecraft) and the electric field from spin-averaged EFW data. The electric field estimates are averaged over the spacecraft. We see that $\mathbf{E} \cdot \mathbf{J}$ is very large for most of the events, generally exceeding the threshold. In general, $\mathbf{E} \cdot \mathbf{J}$ from spin-averaged EFW data is the larger quantity.

Table 2. List of Documented Cluster Reconnection Encounters

Event[a]	Date[b]	T_1[b]	T_2[b]	**X** (R_E)[c]	**Y** (R_E)[c]	**Z** (R_E)[c]	E/P[d]	References[e]
1	2001-08-13	02:55:00	03:00:00	−17	−5.4	−2.7	0.12/0.11	E
2	2001-08-17	16:25:00	16:50:50	−18	−4.9	0.3	0.04/0.05	Ø
3	2001-08-22	09:40:00	10:16:00	−19	−3.4	1.0	0.06/0.07	EBØ
4	2001-08-27	04:03:00	04:07:00	−19	−2.1	−0.2	0.06/0.08	E
5	2001-09-10	07:48:00	08:04:00	−19	2.1	−0.4	0.08/0.11	EBØ
6	2001-09-12	13:05:00	13:24:00	−19	3.0	1.5	0.05/0.07	EB
7	2001-09-15	00:14:00	00:43:00	−19	3.4	0.8	0.08/0.10	E
8	2001-09-15	04:52:30	05:16:00	−19	3.4	−2.7	0.05/0.07	EBØ
9	2001-10-01	09:27:30	10:01:00	−16	7.9	0.9	0.09/0.09	EBØ
10	2001-10-08	12:32:00	13:45:00	−15	9.5	0.2	0.08/0.08	EBØ
11	2001-10-11	03:24:00	03:44:00	−16	10.8	−1.6	0.06/0.10	EBØ
12	2002-08-18	17:00:00	17:36:00	−17	−5.1	3.3	0.01/0.02	EBØ
13	2002-08-21	07:53:50	08:40:00	−18	−4.3	0.0	0.34/0.33	EBØ
14	2002-08-28	10:00:00	10:11:00	−19	−2.3	0.0	0.27/0.22	EB
15	2002-09-13	18:07:00	18:26:00	−17	2.2	2.7	0.08/0.20	BØ
16	2002-09-18	12:57:00	13:53:00	−18	3.8	0.7	0.07/0.16	EB
17	2002-10-02	21:15:00	21:38:00	−17	7.8	−0.1	0.03/0.07	EBØ
18	2002-10-26	09:14:00	09:30:00	−11	11.4	−0.3	0.09/0.32	E
19	2003-08-17	16:20:00	17:20:00	−17	−5.6	3.3	0.22/0.25	B
20	2003-08-24	18:30:00	19:14:00	−17	−3.8	3.1	0.22/0.22	B
21	2003-09-01	04:31:00	04:38:00	−19	−1.6	−1.5	0.20/0.27	E
22	2003-09-19	23:25:00	23:35:00	−17	3.7	0.5	0.21/0.27	EBØ
23	2003-10-02	00:25:00	02:00:00	−17	7.7	−3.5	0.21/0.29	E
24	2003-10-04	06:18:00	06:35:00	−16	7.3	−2.9	0.22/0.28	EB
25	2003-10-09	02:18:00	02:31:00	−16	9.3	−3.1	0.23/0.30	EB
26	2004-09-14	23:00:00	23:08:00	−18	2.1	−0.7	0.15/0.36	EBØ
27	2004-10-03	17:50:00	18:25:00	−15	6.3	1.0	0.08/0.29	E
28	2004-10-11	00:33:00	00:50:00	−15	9.0	−1.1	0.12/0.37	E

[a]Sequential event number.
[b]Date (formatted as year-month-day) and start and stop times of each event.
[c]Location of C1 during the event in GSM coordinates.
[d]Elongation and planarity for the Cluster tetrahedron.
[e]The previous investigations that have discussed the events: E = *Eastwood et al.* [2010], B = *Borg et al.* [2012], and Ø = *Østgaard et al.* [2009].

This is clearly larger than the typical load power density observed by Cluster within the plasma sheet [see *Hamrin et al.*, 2009, Figure 5, panel 2]. We find that the average of $\mathbf{E} \cdot \mathbf{J}$ is 78 pW/m^3 and 120 pW/m^3 for the CIS and EFW estimates, respectively. Using different instruments (CIS and EFW) to estimate the electric field in $\mathbf{E} \cdot \mathbf{J}$, we do not expect that they should give identical results. However, for all events in Table 3 we qualitatively obtain the same result: $\mathbf{E} \cdot \mathbf{J}$ is usually large and positive, and it is generally above the selected threshold of ~20 pW/m^3.

Column 4 of Table 3 contains the ratio (in percent) between the DSI $|E_y J_y|$ contribution and the total $|\mathbf{E} \cdot \mathbf{J}|$ using the CIS electric field only. We see that $E_y J_y$ quite often contributes significantly to the power density. However, there are cases when the $E_y J_y$ is rather small and $E_z J_z$ is instead large (not shown). The $E_x J_x$ contribution (not shown) is always small.

From simulations it is known that the dominant contribution to $\mathbf{E} \cdot \mathbf{J}$ should come from the cross-tail current and reconnection electric field [e.g., *Birn and Hesse*, 2005; *Sitnov and Swisdak*, 2011; *Lapenta et al.*, 2014]. However, it is also known that the magnetotail often flaps, causing a tilt of the cross-tail current sheet. This implies that the dominant direction of the normal of the current sheet could vary substantially in the

Table 3. Properties of the Cluster Reconnection Encounters From Table 2

Event[a]	Max $\mathbf{E}\cdot\mathbf{J}$ (pW/m^3) CIS/EFW[b]	Samples $\mathbf{E}\cdot\mathbf{J}>20$ CIS/EFW[c]	$\lvert E_yJ_y\rvert/\lvert\mathbf{E}\cdot\mathbf{J}\rvert$[d] (%)	Peak $-V_x$[e] (km/s)	Peak $+V_x$[e] (km/s)	$\lvert\nabla\cdot\mathbf{B}\rvert/\lvert\nabla\times\mathbf{B}\rvert$[f] (%)	Corr (E_y) EFW-COD/HIA[g] (% EFW)	E_y^{CIS}/E_y^{EFW} COD/HIA[h] (%)
1	20/27	1/3	12	510 (C3)	1020 (C1)	30	0.74/0.67 (100)	120/62
2	157/459	157/117	28	1110 (C4)	580 (C1)	17	0.71/0.52 (96)	54/11
3	68/168	60/55	33	420 (C4)	970 (C4)	20	0.75/0.71 (97)	40/22
4	20/21	1/1	32	570 (C1)	280 (C4)	34	0.85/0.90 (97)	130/120
5	17/41	0/4	73	330 (C3)	340 (C1)	10	0.73/0.75 (98)	59/61
6	44/61	28/38	125	250 (C3)	880 (C3)	18	0.96/0.93 (90)	99/78
7	102/202	31/21	95	450 (C3)	1160 (C1)	19	0.77/0.70 (86)	89/35
8	105/154	96/51	87	900 (C4)	910 (C1)	14	0.81/0.79 (94)	68/48
9	86/180	87/85	95	500 (C1)	910 (C4)	14	0.78/0.53 (98)	95/39
10	59/99	32/31	81	480 (C1)	520 (C3)	17	0.91/0.89 (99)	100/89
11	35/43	12/18	13	710 (C3)	700 (C1)	13	0.80/0.76 (99)	49/26
12	14/20	0/2	33	460 (C4)	670 (C1)	9	0.47/0.51 (100)	52/45
13	135/185	169/149	90	1250 (C1)	1140 (C1)	22	0.77/0.74 (100)	75/41
14	11/26	0/2	30	430 (C4)	820 (C3)	28	0.74/0.81 (100)	75/69
15	21/45	1/8	79	910 (C3)	730 (C3)	19	0.91/0.91 (100)	71/59
16	38/52	17/38	67	310 (C3)	870 (C1)	16	0.84/0.78 (98)	72/35
17	20/41	0/3	91	350 (C3)	1110 (C1)	19	0.82/0.60 (100)	87/27
18	41/58	17/9	49	460 (C3)	570 (C3)	19	0.90/0.84 (93)	77/52
19	513/689	164/63	33	680 (C4)	750 (C4)	20	NaN/ NaN (98)	NaN/NaN[i]
20	151/166	79/35	76	990 (C4)	620 (C4)	18	NaN/ NaN (92)	NaN/NaN
21	85/7	45/0	91	610 (C3)	250 (C1)	11	0.79/0.85 (100)	190/180
22	61/80	19/7	84	580 (C1)	660 (C1)	11	0.61/0.79 (97)	42/36
23	46/70	26/8	25	110 (C3)	650 (C1)	22	0.81/0.83 (97)	92/82
24	102/86	28/18	17	290 (C1)	1310 (C1)	40	0.83/0.86 (98)	50/30
25	79/96	15/16	45	610 (C1)	150 (C1)	29	0.50/0.71 (98)	46/37
26	68/92	12/13	82	820 (C4)	560 (C1)	16	0.68/0.62 (93)	14/15
27	52/128	39/13	100	390 (C4)	420 (C4)	21	0.76/0.79,(93)	80/84
28	46/ 32	25/4	18	410 (C3)	290 (C1)	15	0.81/0.88 (93)	160/120

[a] Event number.
[b] Maximum value of $\mathbf{E}\cdot\mathbf{J}$ using the electric field obtained from CIS and EFW, respectively.
[c] Number of samples with $\mathbf{E}\cdot\mathbf{J}>20$ pW/m^3 for the CIS and EFW estimates.
[d] Median ratio between the DSI E_yJ_y contribution and $|\mathbf{E}\cdot\mathbf{J}|$ using the CIS electric field.
[e] Tailward ($-V_x$) and earthward ($+V_x$) velocity components in GSM. The peaks are calculated as the 2.5 and 97.5 percentiles, respectively. Only data from the spacecraft which observe the largest peaks are shown.
[f] Quality estimate $|\nabla\cdot\mathbf{B}|/|\nabla\times\mathbf{B}|$ (median value) for the curlometer current.
[g] Correlation coefficient between DSI E_y obtained from EFW and from CODIF or HIA on spacecraft C1. The numbers within brackets indicate how many percent of the event has available EFW E_y data on C1.
[h] Median ratio between DSI E_y obtained from EFW and from CODIF or HIA on spacecraft C1.
[i] Missing data have been indicated with NaN (Not a Number).

GSM *yz* plane. In the series of current sheet crossings from 1 October 2001, discussed in *Wygant et al.* [2005], the tilt of the normal was observed to vary between the events. For example, near 09:46:50, the normal had significant contributions in both *y* and *z*. Investigating this event in detail, we find (not shown) that both E_yJ_y and E_zJ_z contribute significantly to $\mathbf{E}\cdot\mathbf{J}$. *Borg et al.* [2005], on the other hand, investigated one reconnection event at ~23:30 UT from 19 September 2003, when the normal to the current sheet was found to be closely aligned with GSM *z*. A detailed analysis of the power density (not shown) shows that the dominant contribution to $\mathbf{E}\cdot\mathbf{J}$ comes from GSM *y*. It is hence reasonable to expect that the relative contribution of E_yJ_y and E_zJ_z (see column 4 in Table 3) to the total $\mathbf{E}\cdot\mathbf{J}$ may indicate the tilt of the cross-tail current sheet. However, in many

cases the analysis is complicated, e.g., due to difficulties in estimating the current sheet normal in a rapidly flapping tail. It is outside the scope of the present article to investigate this further.

In columns 5 and 6 of Table 3, the spacecraft that observe the peak earthward ($+V_x$) and tailward ($-V_x$) plasma flows are presented together with the peak values in km/s. The peaks are computed as the 2.5 and 97.5 percentiles for the earthward and tailward flows, respectively. We clearly see that all documented Cluster reconnection encounters correlate with observations of fast earthward and/or tailward plasma flows, which is expected for reconnection regions.

In column 7 the median for each event of the quality estimate $|\nabla \cdot \mathbf{B}|/|\nabla \times \mathbf{B}|$ of the curlometer current is displayed. For most events this value is smaller than 30%, and we expect that the curlometer would be reliable [*Paschmann and Schwartz*, 2000]. Moreover, the elongation and the planarity are small (see Table 2). This guarantees an approximately equilateral Cluster tetrahedral configuration, which is optimal for the curlometer.

As can be seen from the detailed investigation of the two sample events in Figures 3 and 6, the spin-averaged EFW electric field strongly underestimates the full-resolution electric field measured by EFW, but it still resolves signatures of the normal and perpendicular reconnection electric fields. Moreover, the electric field estimated from the CIS ion moments according to the frozen-in assumption, $-\mathbf{V} \times \mathbf{B}$, often underestimates the magnitude of the spin-averaged EFW electric field. However, the signature of the CIS field correlates well with the spin-averaged EFW field. For the two sample events we hence concluded that the CIS electric field can be used for studying the power density of the reconnection load. Even though the magnitude of the power density is underestimated and the frozen-in condition is not formally valid near the *X* line, CIS qualitatively gives the same result that $\mathbf{E} \cdot \mathbf{J}$ is large and positive.

Correlation coefficients for all 28 documented Cluster reconnection encounters are shown in column 8 of Table 3. The coefficients are computed on spacecraft C1 for the DSI E_y component obtained from spin-averaged EFW data and from the CODIF and HIA ion moments, respectively. The numbers within brackets indicate how many percent of each event has available EFW E_y data on C1 (few EFW samples would indicate a less accurate correlation coefficient). Note that both CODIF and HIA are not operational on C1 for the events 19 and 20 and that there are therefore corresponding NaNs in columns 8 and 9. Averaging over all the 28 events, the E_y correlation coefficients for EFW-CODIF and EFW-HIA are 0.77 and 0.76, respectively, and we conclude that the measurements in general are highly correlated. The correlation coefficient is never smaller than ~0.5, which suggests at least a moderate correlation.

The last column of Table 3 contains the ratio between DSI E_y obtained from CIS (CODIF or HIA) and from spin-averaged EFW (computed in the same way as for the sample events in sections 4.1 and 4.2). For most events, CIS underestimates E_y. On the average, CODIF and HIA observe 80% and 60% of the spin-averaged EFW electric field.

From the above reasonings we conclude that the full-resolution EFW electric field is most optimal for resolving the power density $\mathbf{E} \cdot \mathbf{J}$ of the reconnection load. However, the spin-averaged EFW electric field can also be used even though it underestimates the magnitude of the power density. Moreover, if direct electric field measurements are not available, the electric field estimated from the ion moments is also sufficient, even though it underestimates the magnitude of the power density even more. Note that it is especially remarkable that the CIS estimate (in particular CODIF) resolves the electric field variation so well, even though it underestimates the magnitude. We therefore argue that $\mathbf{E} \cdot \mathbf{J}$ in general can be estimated by using only the CIS electric field, even though the frozen-in condition is not formally satisfied in the vicinity of a reconnection region.

It is worthwhile to note that the events presented in Table 3 are observed by Cluster during four different years, 2001–2004. During these years, the Cluster tetrahedron was approximately equilateral in the magnetotail plasma sheet. However, the scale size varied over the years according to Table 1. The scale size was smallest in 2003 and largest in 2002. Since both $\mathbf{E}$ and $\mathbf{J}$ in $\mathbf{E} \cdot \mathbf{J}$ are averaged over the Cluster tetrahedron, one would expect that smaller-scale features of $\mathbf{E} \cdot \mathbf{J}$ should be observed in 2003 as compared to 2002 and that the magnitude $|\mathbf{E} \cdot \mathbf{J}|$ would typically be larger in 2003. This can be verified from columns 2 and 3 in Table 3. The average $\mathbf{E} \cdot \mathbf{J}$ using the CIS electric field is 65 pW/m^3 in 2001, 40 pW/m^3 in 2002, 150 pW/m^3 in 2003, and 55 pW/m^3 in 2004. Using the EFW electric field, we similarly find 130 pW/m^3, 61 pW/m^3, 179 pW/m^3, and 84 pW/m^3. Even though the statistics are rather small, we can verify that the power density is on the average approximately 3–4 times larger in 2003 than in 2002. There are also considerably more samples exceeding the

Table 4. Properties of a Set of Additional Events With Large Power Densities

Event[a]	Date[b]	T_1[b]	T_2[b]	X/Y/Z[c] (R_E)	Max $\mathbf{E}\cdot\mathbf{J}$[d] (pW/m^3) CIS/EFW	Samples $\mathbf{E}\cdot\mathbf{J}>20$[e] CIS/EFW	Reconnection?[f]	Comment
1	2001-08-03	10:40	11:15	−17/−8.5/2.2	48/48	38/21	Yes	
2	2001-08-05	13:00	14:10	−17/−7.8/5.7	35/27	6/4	Can be	Several subevents
3	2001-08-07	23:40	00:05	−17/−8.4/2.1	28/38	6/7	Yes	
4	2001-08-12	17:00	18:50	−18/−6.7/3.1	54/47	47/27	Yes	Several subevents
5	2001-08-17	13:00	15:00	−18/−4.7/2.6	114/71	55/77	Can be	Several subevents
6	2001-08-31	17:10	17:20	−19/−0.8/2.5	51/79	9/10	Yes	
7	2001-09-02	23:45	00:35	−19/−0.7/3.5	30/26	2/3	Yes	Several subevents
8	2001-09-07	21:30	22:00	−19/1.2/1.1	21/27	2/4	Yes	
9	2001-09-12	15:10	15:16	−19/2.8/0.5	36/27	3/3	Yes	
10	2001-09-15	03:49	04:35	−19/3.5/−2.0	56/47	44/10	Yes	Several subevents
11	2001-09-24	00:10	00:20	−14/3.4/ 7.2	30/NaN	5/–	Can be	
12	2001-09-26	22:20	23:10	−18/7.1/−0.4	25/59	2/7	No	
13	2001-10-01	11:40	11:50	−17/8.0/−0.4	26/49	17/24	Can be	
14	2001-10-08	14:40	14:50	−16/9.7/−0.3	28/24	2/2	Can be	

[a]Event number.
[b]The date (formatted as year-month-day) and start and stop times.
[c]The event location in GSM coordinates.
[d]The maximum value of $\mathbf{E}\cdot\mathbf{J}$ using the electric field obtained from CIS and EFW, respectively.
[e]The number of samples with $\mathbf{E}\cdot\mathbf{J}>20$ pW/m^3 for the CIS and EFW estimates.
[f]Whether or not signatures of reconnection are seen.

~20 pW/m^3 threshold (both for CIS and EFW) in 2003 than in 2002. However, when comparing results from different years, it should also be remembered that the instruments may deteriorate with age and that this can cause additional errors.

5.2. Additional Reconnection Events From 2001

As a complement to the statistics discussed above, we have also automatically scanned through the plasma sheet data from 2001 within the region $X < -10R_E$ and $|Y| < 10R_E$ to identify events with $\mathbf{E}\cdot\mathbf{J} > 20$ pW/m^3 using the CIS electric field. For the event selection we have also required that all spacecraft observe densities larger than 0.01 cm^{-3} (e.g., it is likely that no spacecraft is in the lobe) and that both the elongation and the planarity are smaller than 0.4. All selected events have been inspected visually to define their start and stop times to include the strong $\mathbf{E}\cdot\mathbf{J}$ signatures as well as any significant flows or flow reversals. All identified events (except the ones that are already presented in Tables 2 and 3) are listed in Table 4. In total, there are 14 such additional events from 2001 that satisfy the selection criteria. However, note that some of these events may include several subevent fulfilling the criteria.

The events in Table 4 have been analyzed manually to conclude whether or not they are likely to be associated with reconnection (see column 8 in Table 4). To associate an event with reconnection, as a general rule we have used a requirement that there is at least 400 km/s jets within a time interval of 2 min surrounding the event. This is reasonable, since reconnection jets with speeds comparable to the Alfvén speed (~800 km/s for a magnetic field of ~20 nT and a plasma density of ~0.3 cm^{-3}) would be expected in the case of ongoing reconnection, unless the spacecraft are located close to the diffusion region or in the jet braking region. Jet speeds can be lower when a spacecraft is very close to the diffusion region or in the jet braking region. In the case of lobe reconnection, on the other hand, Alfvén speed can be even higher due to the low plasma density in lobes. As an additional test for an event to be associated with reconnection, we have checked for the presence of Hall magnetic field signatures. As a general trend we expect that all three components B_x, B_y, and V_x are either positive or any two of them are negative if a spacecraft is on the outer edges of the tail current sheet.

From Table 4 we see that only one of the 14 events is clearly not related to reconnection. Most of the other events show signatures of reconnection, but a few events are difficult to classify.

In Table 4 we have only included events from 2001 which fulfill our selection criteria (but which are not already listed in Tables 2 and 3). A similar selection method based on $\mathbf{E} \cdot \mathbf{J} > 20$ pW/m^3 can be used for selecting events also from 2002–2004. However, during later years, the instruments deteriorated, and more care is needed to separate signals from the background variations. It is outside the scope of the present article to include a full list of events also from 2002–2004.

6. Summary and Discussion

We have studied the capability of using Cluster data for analyzing energy conversion at ion scales in the vicinity of magnetotail reconnection by computing the power density, $\mathbf{E} \cdot \mathbf{J}$. In particular, we have investigated the use of $\mathbf{E} \cdot \mathbf{J}$ for identifying possible reconnection events from large sets of observed data. $\mathbf{E}$ is the electric field averaged over the spacecraft, and $\mathbf{J}$ is the current density estimated with the curlometer method from multispacecraft measurements of the magnetic field. For our analysis, we have used direct electric field measurements from the EFW instrument as well as estimates from the CIS ion moments through the frozen-in condition ($-\mathbf{V} \times \mathbf{B}$).

The power density probes the energy transfer between the particles and the field. For example, when $\mathbf{E} \cdot \mathbf{J} > 0$ energy is transferred from the magnetic field to the plasma (in the form of bulk motion and heating) if the Poynting flux can be neglected. Such a load process is expected in the vicinity of a reconnection site, where magnetic energy is used for accelerating plasma jets. In practice we have used $\mathbf{E} \cdot \mathbf{J}$ only as a qualitative measurement of the energy conversion, and we have argued that a large and positive value of $\mathbf{E} \cdot \mathbf{J}$ indicates that an event is likely to be associated with reconnection. Using some simple theoretical arguments, we have shown that a suitable $\mathbf{E} \cdot \mathbf{J}$ threshold for magnetotail reconnection is $\sim$ 20 pW/m^3 ($X < -10R_E$ and $|Y| \lesssim 10R_E$). The exact magnitude of the power density depends on the scale size of the measurements (higher-resolution data resolve smaller-scale signatures). The $\mathbf{E} \cdot \mathbf{J}$ threshold must hence be adjusted to the resolution of the measurements.

The power density should consequently only be used as a primary indicator of potential reconnection regions, and the threshold for identifying the events must be adjusted to the resolution of the measurements. Moreover, the selected events must be reviewed separately to confirm any possible reconnection signatures by looking for other signatures in the data such as reconnection jets, Hall electric and magnetic fields, and guide fields [e.g., *Eastwood et al.*, 2010].

By using Cluster data from 2001–2004, we have analyzed two sample events in detail and conducted two statistical investigations, and we have shown that $\mathbf{E} \cdot \mathbf{J} \gtrsim 20$ pW/m^3 indeed is a very good indication of likely magnetotail reconnection, even though there is no absolute one-to-one correlation between the magnitude of $\mathbf{E} \cdot \mathbf{J}$ and reconnection signatures.

It is well known that the power density can be large and positive not only in the vicinity of reconnection but also in other regions of space, e.g., at dipolarization fronts [*Hamrin et al.*, 2014; *Huang et al.*, 2015]. *Huang et al.* [2015] conducted investigations of energy conversion at dipolarization fronts as observed by Cluster in 2003. They used high-resolution FGM magnetic field data (23 Hz) and EFW electric field data (25 Hz) to compute $\mathbf{E} \cdot \mathbf{J}$, and they found that the power density at dipolarization fronts at times can be as high as several hundred pW/m^3. However, how large power density we actually can observe with our spacecraft instruments depends on the amount of energy converted between the particles and the fields and also on the scale size of the regions of interest (as compared to the scale size of the measurements). In this article we have focused on studying energy conversion at ion scales, and we have used measurements averaged over the Cluster tetrahedron (multispacecraft data) and 4 s resolution data. Using single-spacecraft and high time resolution data will of course better resolve small-scale features in the power density than when using spatially averaged and low-resolution data.

One limiting factor when computing $\mathbf{E} \cdot \mathbf{J}$ is the method for estimating the current density, $\mathbf{J}$. Using a single-satellite method, small-scale signatures can be resolved, but it requires additional information (e.g., the existence of clear current sheets and the knowledge of their orientation and motion) which sometimes is difficult to obtain. The multispacecraft curlometer method, on the other hand, is more general and is simple to implement, but it tends to smooth the resulting current density (and it is only applicable when the

Cluster tetrahedron is approximately equilateral). We argue that the curlometer method is most useful when automatically scanning large data sets with the aim of finding potential reconnection regions. However, when investigating the energy conversion at single reconnection events, a single-satellite method for the current density might be more useful.

We have computed $\mathbf{E} \cdot \mathbf{J}$ using $\mathbf{E}$ both from direct electric field measurements (from EFW) and from derived quantities $\mathbf{E} = -\mathbf{V} \times \mathbf{B}$ (from CIS). We have shown that both methods qualitatively give the same result with large and positive values of the power density in the vicinity of reconnection, even though CIS generally underestimates the magnitude (since the frozen-in assumption is not formally valid in the diffusion region near an *X* line). If possible, electric fields obtained from direct measurements should therefore be used when computing $\mathbf{E} \cdot \mathbf{J}$ near a reconnection site. However, we have shown that approximate fields obtained from ion moments can be used whenever direct electric field measurements are not available. Being able to use ion moments instead of direct electric field measurements of course facilitates any investigation where one cannot obtain the full electric field by direct measurements. This is often the case for Cluster in the magnetotail, since the EFW instrument only measures the field in the satellites' spin planes and computes the third component by assuming $\mathbf{E} \cdot \mathbf{B} = 0$.

In this article we have shown that the power density can be computed from multispacecraft data, and it is rather straightforward to construct an automatized routine, which searches the magnetotail data for events with large and positive power densities. Such events have a high probability to be associated with magnetic reconnection. These events can subsequently be analyzed manually for verification. We hence argue that the power density can be used as a primary indicator for identifying possible reconnection events from large sets of data, e.g., from the Cluster and the MMS missions.

Acknowledgments

We thank the Cluster FGM, CIS, and EFW teams and the Cluster Science Archive, CSA, http://www.cosmos.esa.int/web/csa (previously the Cluster Active Archive, CAA) for providing well-calibrated Cluster magnetic field, electric field, and velocity moments data. M.H. and T.P. acknowledge the support by the grant from the Swedish National Space Board, project 78/11AB. H.G. was supported by the Belgian Science Policy Office through the Solar-Terrestrial Centre of Excellence and by PRODEX/Clustercontract 13127/98/NL/VJ(IC)-PEA 90316.

Michael Liemohn thanks two reviewers for their assistance in evaluating this paper.

References

Anekallu, C. R., M. Palmroth, T. I. Pulkkinen, S. E. Haaland, E. Lucek, and I. Dandouras (2011), Energy conversion at the Earth's magnetopause using single and multispacecraft methods, *J. Geophys. Res.*, *116*, A11204, doi:10.1029/2011JA016783.

Baker, D., et al. (2002), Timing of magnetic reconnection initiation during a global magnetospheric substorm onset, *Geophys. Res. Lett.*, *29*(24), 2190, doi:10.1029/2002GL015539.

Birn, J., and M. Hesse (2005), Energy release and conversion by reconnection in the magnetotail, *Ann. Geophys.*, *23*(10), 3365–3373.

Borg, A. L. (2006), Average properties of the magnetic reconnection ion diffusion region in the Earth's magnetotail: The 2001–2005 Cluster observations and comparison with simulations, PhD thesis, Univ. of Oslo, Oslo, Norway.

Borg, A. L., M. Øieroset, T. D. Phan, F. S. Mozer, A. Pedersen, C. Mouikis, J. P. McFadden, C. Twitty, A. Balogh, and H. Rème (2005), Cluster encounter of a magnetic reconnection diffusion region in the near-Earth magnetotail on September 19, 2003, *Geophys. Res. Lett.*, *32*, L19105, doi:10.1029/2005GL023794.

Borg, A. L., M. G. G. T. Taylor, and J. P. Eastwood (2012), Electron pitch angle distribution during magnetic reconnection diffusion region observations in the Earth's magnetotail, *Ann. Geophys.*, *30*(1), 109–117, doi:10.5194/angeo-30-109-2012.

Burch, J. L., T. E. Moore, R. B. Torbert, and B. L. Giles (2015), Magnetospheric multiscale overview and science objectives, *Space Sci. Rev.*, 1–17, doi:10.1007/s11214-015-0164-9.

Cattell, C., et al. (2005), Cluster observations of electron holes in association with magnetotail reconnection and comparison to simulations, *J. Geophys. Res.*, *110*, A01211, doi:10.1029/2004JA010519.

Chen, L. J.et al. (2008), Observation of energetic electrons within magnetic islands, *Nat. Phys.*, *4*(1), 19–23, doi:10.1038/nphys777.

Daughton, W., J. Scudder, and H. Karimabadi (2006), Fully kinetic simulations of undriven magnetic reconnection with open boundary conditions, *Phys. Plasmas*, *13*(7), 072101, doi:10.1063/1.2218817.

Daughton, W., V. Roytershteyn, B. J. Albright, H. Karimabadi, L. Yin, and K. J. Bowers (2009), Influence of Coulomb collisions on the structure of reconnection layers, *Phys. Plasmas*, *16*(7), 072117, doi:10.1063/1.3191718.

Dungey, J. (1961), Interplanetary magnetic field and auroral zones, *Phys. Rev. Lett.*, *6*(2), 47–48, doi:10.1103/PhysRevLett.6.47.

Dunlop, M. W., and J. P. Eastwood (2008), The curlometer and other gradient based methods, in *Multi-spacecraft Analysis Methods Revisited*, vol. 8, edited by D. Paschmann, pp. 17–26, ISSI Scientific Reports Series, ESA Communications, Noordwijk, Netherlands.

Dunlop, M. W., A. Balogh, K. H. Glassmeier, and P. Robert (2002), Four-point Cluster application of magnetic field analysis tools: The Curlometer, *J. Geophys. Res.*, *107*(A11), 1384, doi:10.1029/2001JA005088.

Eastwood, J., D. Sibeck, J. Slavin, M. Goldstein, B. Lavraud, M. Sitnov, S. Imber, A. Balogh, E. Lucek, and I. Dandouras (2005), Observations of multiple *X*-line structure in the Earth's magnetotail current sheet: A Cluster case study, *Geophys. Res. Lett.*, *32*, L11105, doi:10.1029/2005GL022509.

Eastwood, J. P., T.-D. Phan, F. S. Mozer, M. A. Shay, M. Fujimoto, A. Retinò, M. Hesse, A. Balogh, E. A. Lucek, and I. Dandouras (2007), Multi-point observations of the Hall electromagnetic field and secondary island formation during magnetic reconnection, *J. Geophys. Res.*, *112*, A06235, doi:10.1029/2006JA012158.

Eastwood, J. P., T. D. Phan, M. Øieroset, and M. A. Shay (2010), Average properties of the magnetic reconnection ion diffusion region in the Earth's magnetotail: The 2001–2005 Cluster observations and comparison with simulations, *J. Geophys. Res.*, *115*, A08215, doi:10.1029/2009JA014962.

Egedal, J., W. Fox, N. Katz, M. Porkolab, M. Øieroset, R. P. Lin, W. Daughton, and J. F. Drake (2008), Evidence and theory for trapped electrons in guide field magnetotail reconnection, *J. Geophys. Res.*, *113*, A12207, doi:10.1029/2008JA013520.

Egedal, J., W. Daughton, J. F. Drake, N. Katz, and A. Lê (2009), Formation of a localized acceleration potential during magnetic reconnection with a guide field, *Phys. Plasmas*, *16*(5), 050701, doi:10.1063/1.3130732.

Egedal, J., N. Katz, J. Bonde, W. Fox, A. Le, M. Porkolab, and A. Vrublevskis (2011), Spontaneous onset of magnetic reconnection in toroidal plasma caused by breaking of 2D symmetry, *Phys. Plasmas*, *18*(11), 111203, doi:10.1063/1.3626837.

Egedal, J., A. Le, and W. Daughton (2013), A review of pressure anisotropy caused by electron trapping in collisionless plasma, and its implications for magnetic reconnection, *Phys. Plasmas*, *20*(6), 061201, doi:10.1063/1.4811092.

Eriksson, S., M. Øieroset, D. Baker, C. Mouikis, A. Vaivads, M. Dunlop, H. Reme, R. Ergun, and A. Balogh (2004), Walen and slow-mode shock analyses in the near-Earth magnetotail in connection with a substorm onset on 27 August 2001, *J. Geophys. Res.*, *109*, A10212, doi:10.1029/2004JA010534.

Escoubet, C. P., R. Schmidt, and M. L. Goldstein (1997), Cluster—Science and mission overview, *Space Sci. Rev.*, *79*, 11–32, doi:10.1023/A:1004923124586.

Escoubet, C. P., M. Fehringer, and M. Goldstein (2001), The Cluster mission—Introduction, *Ann. Geophys.*, *19*(10-12), 1197–1200.

Fu, H. S., et al. (2013), Dipolarization fronts as a consequence of transient reconnection: In situ evidence, *Geophys. Res. Lett.*, *40*, 6023–6027, doi:10.1002/2013GL058620.

Giovanelli, R. (1946), A theory of chromospheric flares, *Nature*, *158*(4003), 81–82, doi:10.1038/158081a0.

Hamrin, M., O. Marghitu, K. Ronnmark, B. Klecker, M. Andre, S. Buchert, L. M. Kistler, J. McFadden, H. Reme, and A. Vaivads (2006), Observations of concentrated generator regions in the nightside magnetosphere by Cluster/FAST conjunctions, *Ann. Geophys.*, *24*(2), 637–649.

Hamrin, M., P. Norqvist, O. Marghitu, S. Buchert, B. Klecker, L. M. Kistler, and I. Dandouras (2009), Occurrence and location of concentrated load and generator regions observed by Cluster in the plasma sheet, *Ann. Geophys.*, *27*, 4131–4146, doi:10.5194/angeo-27-4131-2009.

Hamrin, M., O. Marghitu, P. Norqvist, S. Buchert, M. Andre, B. Klecker, L. M. Kistler, and I. Dandouras (2011), Energy conversion regions as observed by Cluster in the plasma sheet, *J. Geophys. Res.*, *116*, A00K08, doi:10.1029/2010JA016383.

Hamrin, M., et al. (2013), The evolution of flux pileup regions in the plasma sheet: Cluster observations, *J. Geophys. Res. Space Physics*, *118*, 6279–6290, doi:10.1002/jgra.50603.

Hamrin, M., et al. (2014), Evidence for the braking of flow bursts as they propagate toward the Earth, *J. Geophys. Res. Space Physics*, *119*, 9004–9018, doi:10.1002/2014JA020285.

Huang, S. Y., et al. (2015), Electromagnetic energy conversion at dipolarization fronts: Multispacecraft results, *J. Geophys. Res. Space Physics*, *120*, 4496–4502, doi:10.1002/2015JA021083.

Kubyshkina, D. I., D. A. Sormakov, V. A. Sergeev, V. S. Semenov, N. V. Erkaev, I. V. Kubyshkin, N. Y. Ganushkina, and S. V. Dubyagin (2014), How to distinguish between kink and sausage modes in flapping oscillations?, *J. Geophys. Res. Space Physics*, *119*, 3002–3015, doi:10.1002/2013JA019477.

Lapenta, G., M. Goldman, D. Newman, S. Markidis, and A. Divin (2014), Electromagnetic energy conversion in downstream fronts from three dimensional kinetic reconnection, *Phys. Plasmas*, *21*, 055702, doi:10.1063/1.4872028.

Nakamura, R., et al. (2002), Fast flow during current sheet thinning, *Geophys. Res. Lett.*, *29*(23), 2140, doi:10.1029/2002GL016200.

Østgaard, N., K. Snekvik, A. L. Borg, A. Asnes, A. Pedersen, M. Øieroset, T. Phan, and S. E. Haaland (2009), Can magnetotail reconnection produce the auroral intensities observed in the conjugate ionosphere?, *J. Geophys. Res.*, *114*, A06204, doi:10.1029/2009JA014185.

Paschmann, G., and S. Schwartz (2000), ISSI Book on Analysis Methods for Multi-Spacecraft Data, in *Proceedings of the Cluster-II Workshop Multiscale/Multipoint Plasma Measurements, ESA Special Publications*, vol. 449, edited by R. A. Harris, Eur. Space Agency, Paris.

Paschmann, G., B. Sonnerup, I. Papamastorakis, N. Sckopke, G. Haerendel, S. Bame, J. Asbridge, J. Gosling, C. Russell, and R. Elphic (1979), Plasma acceleration at the earths magnetopause—Evidence for reconnection, *Nature*, *282*(5736), 243–246, doi:10.1038/282243a0.

Petschek, H. E. (1964), Magnetic field Annihilation, in *Physics of Solar Flares*, edited by W. N. Hess, pp. 425–439, NASA Spec. Publ. 50, Washington, D. C.

Retino, A., et al. (2008), Cluster observations of energetic electrons and electromagnetic fields within a reconnecting thin current sheet in the Earth's magnetotail, *J. Geophys. Res.*, *113*, A12215, doi:10.1029/2008JA013511.

Rosenqvist, L., S. Buchert, H. Opgenoorth, A. Vaivads, and G. Lu (2006), Magnetospheric energy budget during huge geomagnetic activity using Cluster and ground-based data, *J. Geophys. Res.*, *111*, A10211, doi:10.1029/2006JA011608.

Rosenqvist, L., H. J. Opgenoorth, L. Rastaetter, A. Vaivads, I. Dandouras, and S. Buchert (2008a), Comparison of local energy conversion estimates from Cluster with global MHD simulations, *Geophys. Res. Lett.*, *35*, L21104, doi:10.1029/2008GL035854.

Rosenqvist, L., A. Vaivads, A. Retinò, T. Phan, H. J. Opgenoorth, I. Dandouras, and S. Buchert (2008b), Modulated reconnection rate and energy conversion at the magnetopause under steady IMF conditions, *Geophys. Res. Lett.*, *35*, L08104, doi:10.1029/2007GL032868.

Runov, A., et al. (2003), Current sheet structure near magnetic *X*-line observed by Cluster, *Geophys. Res. Lett.*, *30*(11), 1579, doi:10.1029/2002GL016730.

Sergeev, V. A., D. A. Sormakov, S. V. Apatenkov, W. Baumjohann, R. Nakamura, A. V. Runov, T. Mukai, and T. Nagai (2006), Survey of large-amplitude flapping motions in the midtail current sheet, *Ann. Geophys.*, *24*, 2015–2024, doi:10.5194/angeo-24-2015-2006.

Sitnov, M. I., and M. Swisdak (2011), Onset of collisionless magnetic reconnection in two-dimensional current sheets and formation of dipolarization fronts, *J. Geophys. Res.*, *116*, A12216, doi:10.1029/2011JA016920.

Snekvik, K., E. Tanskanen, N. Østgaard, L. Juusola, K. Laundal, E. I. Gordeev, and A. L. Borg (2012), Changes in the magnetotail configuration before near-Earth reconnection, *J. Geophys. Res.*, *117*, A02219, doi:10.1029/2011JA017040.

Speiser, T. W. (1965), Particle trajectories in model current sheets 1: Analytical solutions, *J. Geophys. Res.*, *70*, 4219–4226, doi:10.1029/JZ070i017p04219.

Volwerk, M., et al. (2013), Comparative magnetotail flapping: An overview of selected events at Earth, Jupiter and Saturn, *Ann. Geophys.*, *31*, 817–833, doi:10.5194/angeo-31-817-2013.

Wei, X. H., J. B. Cao, G. C. Zhou, O. Santolik, H. Reme, I. Dandouras, N. Cornilleau-Wehrlin, E. Lucek, C. M. Carr, and A. Fazakerley (2007), Cluster observations of waves in the whistler frequency range associated with magnetic reconnection in the Earth's magnetotail, *J. Geophys. Res.*, *112*, A10225, doi:10.1029/2006JA011771.

Wygant, J. R., et al. (2005), Cluster observations of an intense normal component of the electric field at a thin reconnecting current sheet in the tail and its role in the shock-like acceleration of the ion fluid into the separatrix region, *J. Geophys. Res.*, *110*, A09206, doi:10.1029/2004JA010708.

Yamada, M., R. Kulsrud, and H. Ji (2010), Magnetic reconnection, *Rev. Mod. Phys.*, *82*, 603–664, doi:10.1103/RevModPhys.82.603.